Eng. Sci., 2022, **20**, 144–156

Engineered Science

DOI: https://dx.doi.org/10.30919/es8d750

Novel Test Cell for Overall and Spatial Mechanical Analysis of Sheet Molding Compound Composite Part in View of Heterogeneity

Christian Hopmann,[1] Hao Wang,[2,*] Markus Breiing,[2] Kai Fischer,[1, 2] Michael Emonts[2] and Jian Wang[3]

Abstract

Sheet molding compound (SMC) is widely used due to multiple advantages, *e.g.*, low material cost, short production cycle, and ability to adjust the formulation. However, the manufactured SMC parts exhibit spatial property variations in heterogeneity and anisotropy, induced during raw material manufacturing and compression molding. To overall and spatially characterize the SMC part performance with consideration of the local morphology, a test cell was developed, consisting of a mechanical test bench and an optical measurement system. Displacement and force control modes were customizable realized on the test bench with adjustable test parameters. Different load cases and tests were integrated, like a cantilever, three- and four-point bending, creep, and endurance. The overall part geometry, deformation, and full field surface strain could be provided. Furthermore, one unique platform for the real-time finite element analysis of the SMC part performance was developed and integrated. In the exemplary case studies, the functionalities of this test bench were demonstrated based on bending, creep, and endurance test on three-dimensional SMC parts. The parts showed varied bending stiffness with spatially significant heterogeneity. Different creep stages were identified, and local stiffer areas under high stress were prone to creep.

Keywords: Sheet molding compound; Mechanical test; Heterogeneity; Part deformation; Surface strain.
Received: 11 March 2022; Revised: 29 June 2022; Accepted: 11 July 2022.
Article type: Research article

1. Introduction

In recent years, composites with high mechanical properties and low density are required and being used more and more to reduce vehicle weight due to the increasingly stringent emission standards in the automotive and transportation industries.[1] One of the most used composite processing methods is the so-called Sheet molding compound (SMC), which traditionally consists of discontinuous random glass or carbon fiber tows, that are impregnated with vinyl ester or polyester resin.[2] SMC shows a variety of advantages, *e.g.*, low material cost, short curing time, and ability to adjust the formulation.[3] A high mass of SMC were produced in 2018 in Europe, concerning the total production volume of glass fiber reinforced plastic, a share of almost 20%,[4] which shows the importance of this material.

SMC parts are usually manufactured by compression molding,[5,6] which means after stacking the plies of SMC with desired charge geometry and weight into a preheated lower tool, the upper tool is brought down under a certain closing speed to squeeze the SMC charge and to force flowing to fill the mold cavity. Furthermore, during compression molding, the charge is subjected to heating, chemical reaction, and cooling with microstructure development and induced internal stresses. The aforementioned mechanisms are heterogeneous and strongly affect the final SMC part properties.[7] Generally, the SMC parts are characterized by high cost specific mechanical properties, geometrical complexity, and short manufacturing time for large-scale production.[6]

However, SMC parts exhibit property variations in anisotropy and heterogeneity,[8,12] which is critical to structural components. Generally, anisotropy is generated during manufacturing SMC raw material by the random orientation of dropped fibers on the moved conveyor belt and during compression molding due to the flow-induced fibe

[1] *Institute for Plastics Processing (IKV), RWTH Aachen University, Aachen 52074, Germany.*
[2] *Aachen Center for Integrative Lightweight Production of RWTH Aachen University (AZL), Aachen 52074, Germany.*
[3] *College of Mechanical and Electrical Engineering, Beijing University of Chemical Technology, Beijing 100029, China.*
**E-mail:* hao.wang@azl.rwth-aachen.de (H.Wang)

orientation.[3,13-17] Furthermore, due to manufacturing variation, the raw SMC material could possess spatially different fiber volume content,[18] which could also be caused by fiber matrix separation during compression molding.[19,20] All these factors lead to heterogeneity in the final part.

Trauth *et al.* investigated the tension behavior of SMC material in different directions concerning conveyor movement direction and different fiber volume content.[13] They pointed out that the SMC material presented slight anisotropy, which increased with a higher fiber volume content. Shirinbayan compared the tension behavior of randomly oriented (RO) and highly oriented (HO) SMC plates with respect to parallel (HO-0°) and perpendicular to the mold flow direction (HO-90°).[3] It is figured out that Young's modulus and failure stress of HO-0° samples were pronounced higher than that of HO-90° and RO samples.

As above-mentioned, the properties of SMC samples are widely characterized at coupon level in the parallel direction and perpendicular direction to the mold flow, according to corresponding standards to indicate the property variations.[19,21-22] However, only limited work was focused on characterizing the mechanical property variations on part level. Martulli et al. characterized one thick-walled SMC chassis part using a bending test to evaluate the influence of manufacturing parameters on part performance, where force and displacement were recorded to calculate the global part rigidity.[23] Similarly, Oldenbo et al. investigated the influence of fiber orientation on the global stiffness of an automotive engine hood, which was calculated using the resulting maximum deflection under a specific loading force.[24] In the above test, the single measured values were unable to describe and observe the overall part performance and the related spatial variations. Due to the variations, the SMC parts are designed with a very conservative tolerance and are normally constructed with isotropic material property, which leads to an overdesign with a high safety factor from three to five.[25,26]

An improved design to reduce the uncertainties requires a better understanding of the spatial property distribution and the process-induced causes. Currently, this is costly to implement since the samples have to be taken and tested locally with high granularity. To determine the spatial mechanical properties, *e.g.*, stiffness, with consideration of the local morphology, a new test methodology based on applying different elastic deformation modes is being developed. For its implementation, a novel test cell is designed and introduced in the present work. It consists of a test bench to apply various loading and deformation modes on SMC parts and an optical measurement system to observe the overall part geometry, deformation, and strain under external loads. The test cell, including configuration, testing programs, and analyzable measured values are introduced. Under the cantilever test, the SMC parts' bending property, creep behavior, and endurance performance are globally and locally characterized using deformation and surface strain.

2. Novel test cell

2.1 Design of test cell

The test cell consists of two main units, which are schematically and physically depicted in Fig. 1and Fig. S1, respectively. A test bench applies diverse loading modes on the part, and an optical measurement system observes the overall part geometry, deformation, and strain under loading.

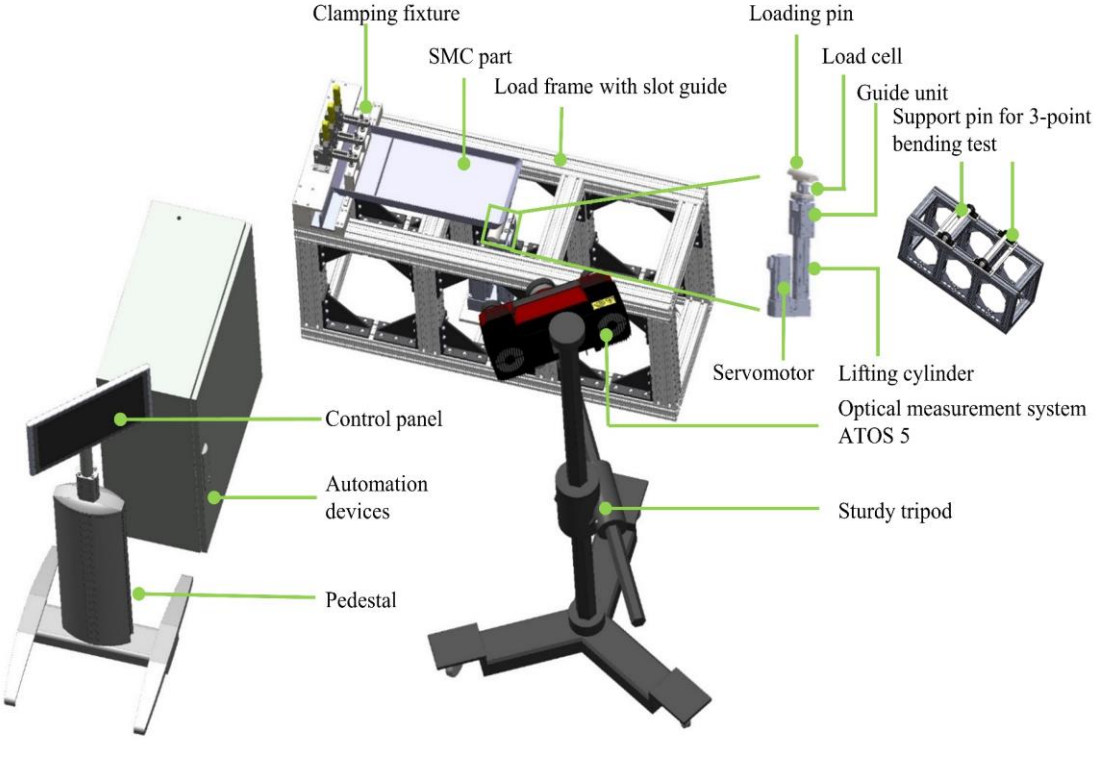

Fig. 1 Schematic diagram of the test cell.

The basic configuration of the test bench is composed of a load frame, clamping fixture for cantilever test, support pins for 3- and 4-point bending test, lifting cylinder with guide unit, servomotor, load cell, and loading pin, as well as automation devices. The load frame, made of die-casting Aluminum alloy, is the structure-giving assembly of the test bench and takes the loads generated by tests. Thanks to the slot guides in the load frame, the clamping fixture could be positioned flexibly to easily fasten the parts, which provides a variable clamping force up to 11,100 N. For the 3-point bending test, the support pins with a radius of 25 mm are positioned in rolling bearing housings to reduce friction between pin and test object during the relative movement. The bending is generated by the linear movement of an electric cylinder, which is driven by a servomotor via a belt transmission. The cylinder could provide a 300 mm hub and a maximum feed force of 5,000 N with a maximum twisting angle of 0.15 degrees. To increase the maximum sustainable radial force on the cylinder drive shaft, a guide unit is implemented and assembled on the cylinder. The load cell (S9M, Hottinger Baldwin Messtechnik GmbH, Germany) with a nominal force in a range of 5,000 N is positioned between the guide unit and loading pin, which achieves the accurate experimental loading force with a linearity deviation of 0.02%. The loading pin has the same radius as the support pins.

The automation devices, including a control cabinet, such as industrial PC, servo amplifier, safety card, various terminals, *etc*., are supplied by Beckhoff Automation GmbH & Co. KG, Germany. To implement the management of the sub-components and the automation controlling functions, such as PLC (Programmable Logic Controller), field devices, and input/output management, the TwinCAT (The Windows Control and Automation Technology), a run-time control system from Beckhoff, was applied. A Unity middleware was employed to access TwinCAT to monitor the test status, sample, and record data. In addition, this middleware serves as an interactive graphical HMI (Human-Machine Interface) to define the test parameters and display the test results in real-time.

The optical measurement system is the ATOS 5 (GOM GmbH, Germany), consisting of two 8 Mega Pixel CMOS (complementary metal oxide semiconductor) Cameras with a resolution of 3357 × 2456 Pixel. ATOS 5 works according to the Triple Scan Principle with narrow-band blue light.[27] Fringe patterns are projected on the scanned object to build up the point clouds, which are transferred together utilizing reference points to compute the 3D object surface. A number of parts could be fully digitalized due to the large measurement volume of 700 × 530 mm, which can be enlarged by using common reference points during scanning. Furthermore, the ATOS 5 provides high accuracy. A deviation of maximal 11 µm for the length of 320 mm and a deviation of maximal 6 µm for the sphere with a diameter of 40 mm were achieved on acceptance to VDI/VDE 2634.[28] To realize measurements in different views, the ATOS 5 is mounted on a sturdy tripod with a swivel head, moving freely in five-axis space.

2.2 Diverse test programs and analyzable measured value

To apply diverse loading and deformation modes on the test object, multiple kinds of test programs and functions are not only manually but also automatically executed at the test cell, such as displacement- and force-control mode with different configurable test parameters to study the part behavior, *e.g.*, preload force and velocity, expected displacement and force, feeding velocity, as well as the loading cycle and delay time, *etc*. The test process, parameters, and the sensor values of force, displacement, and velocity are fully monitored and displayed in real-time in the HMI. The raw test data of the whole test procedure, namely preloading, loading, delay, and unloading, is fully documented in a before-defined workspace for future post-processing.

Thanks to the customized test programs, the creep behavior of the SMC part under different deformation modes can be investigated by defining the test parameter, "delay time." After reaching the expected displacement or force, the servomotor and cylinder stop moving and keep the status. Meanwhile, the force values in the specific delay time are recorded. In addition, by setting the parameter, "cycle," the durability behavior of the SMC part can be analyzed. That is, the SMC part is subjected to repeated loading and unloading procedures until reaching the set loading cycles.

In addition to the measured values by test bench, the overall part geometry is contactless measured with the software ATOS Professional (GOM GmbH, Germany) through the optical measurement system. The overall and spatial part deformation can be analyzed by comparing the measured data with the CAD model. Furthermore, with the aid of the software Aramis Professional (GOM GmbH, Germany), the full field part surface strain and movement in the in- and out-of-plane direction are quantified. To reduce the influence of environmental variation on the measurement results, the load frame of the test bench can be exemplarily set as a rigid body to compensate for the variation. Using inspection functions of that software, the overall and spatial strain distribution in different directions on the part and along different paths are accessible.

2.3 Integrated platform for inline finite element analysis

Furthermore, a unique platform was developed and integrated into the middleware for the Abaqus (Dassault Systèmes SE, France) solver to realize a real-time finite element analysis to virtually investigate and present the overall and spatial mechanical behavior of the part, besides the single measured value by the test bench. The architecture of the platform and the procedures are illustrated in Fig. 2a and described in the following. The Abaqus could be connected with the middleware via C#/.NET and homemade Python scripts on the same PC or remotely. After connecting, the generated protocol file of a flexural test by the middleware could be manually (get from file) or automatically (get the last piece) sent to Abaqus

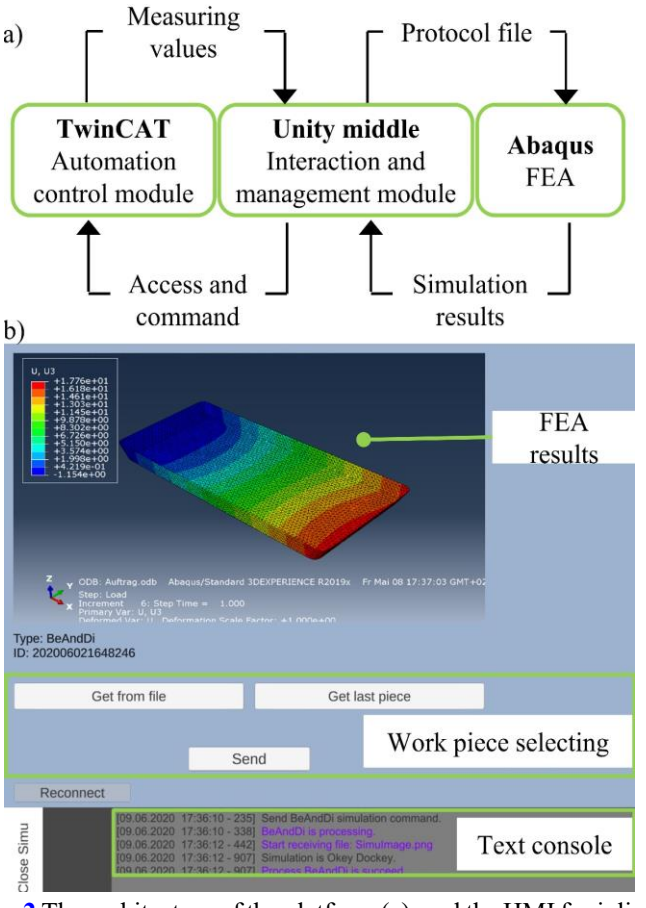

Fig. 2 The architecture of the platform (a), and the HMI for inline-simulation (b).

via the button "Send," as shown in Fig. 2b. The measured force will be extracted and defined as input for the structural simulation. The part performance will be simulated with the predefined and embedded boundary conditions and material cards in MATLAB and Python scripts. After simulation, the corresponding results (the odb-output file; displacement, strain, *etc*. in image format) are immediately sent back to the middleware to provide the inspector with the whole part performance. The illustrated simulation result in Fig. 2b was a part deformation under the cantilever test. The connection status, data transfer, and communication information are real-time displayed in the text console. Since this work does not focus on finite element analysis, the boundary conditions for simulation and the implemented material cards with local fiber orientation are not further discussed.

3. Exemplary case study

3.1 Experimental

3.1.1 Manufacturing samples

The samples were made of one industry-grade Sheet molding compound, which is specified for automotive applications on (semi-) structural components, consisting of an unsaturated polyester resin matrix and chopped glass fiber bundles (weight content of 35% and fiber length about 25 mm). To avoid inconstant sheet geometry and reduce the caused influence on the final part performance, one template made of steel was used to cut the raw material roll in sheets with the dimensions of approximately 513.5 × 234 mm. The sheets were cut along the direction of the conveyor belt to ensure reproducibility and traceability. After stacking three sheets on top of each other, the charge was placed in the center of the mold core at 135 °C (recommendation of the raw material supplier) with a mold coverage of 65% (Fig. 3a), which was integrated into a commercial industrial hydraulic press with a clamping force up to 18,000 KN (Schuler Pressen GmbH, Germany) (Fig. 3b). The charge was compression molded with a closing speed of 5 mm/s under an increased press force until 2,100 KN (about 100 bar).[20,29] After that, the press switched automatically from speed control mode to force control mode, and the SMC was cured 300 seconds under the force, while the mold cavity had a higher temperature of 150 °C to avoid any collision with the mold core due to the overlapping edge. In total, 26 parts were manufactured with a dimension of 695 × 300 × 50 mm (Fig. 3c).

3.1.2 Sample characterization

To exemplify the novel test cell, diverse experiments were carried out to characterize the SMC part in terms of spatial and overall mechanical properties. The force control mode was first implemented in this work to characterize the bending behavior by employing the cantilever test. The test procedure was divided into the following steps. First, the part was fastened on the test bench with the clamping fixture and loaded with a preload of 5 N at a speed of 0.5 mm/s. The corresponding cylinder position was set to "0". The part was

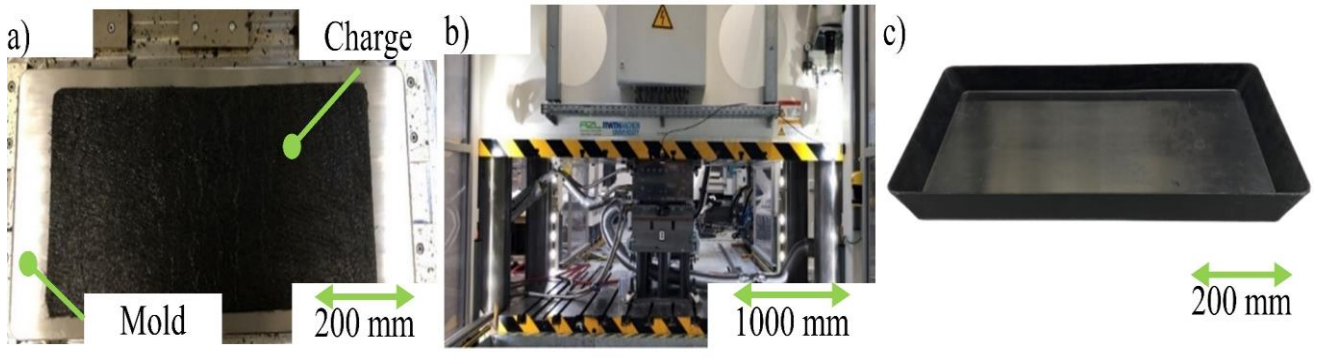

Fig. 3 SMC charge on the mold (a), compression molding with a commercial, industrial hydraulic 18,000 kN press (b), the final SMC part (c).

entirely scanned by ATOS 5, and the resulting geometry was defined as the starting value. Subsequently, the part was loaded up to 155 N (determination of the loading force is given in Fig. S2) at the same test speed. The corresponding cylinder position was designated as the final position. The part was re-recorded by ATOS 5, and the related geometry was defined as the end value. During the measurement, the cylinder did not move. After recording, the part was unloaded immediately and returned to the initial position.

The difference between the starting and end values was taken to calculate the part deformation under the given load. The loaded SMC part is shown in Fig. 4a. A detailed description of the test conditions is illustrated in Fig. 4b. To study the SMC part heterogeneity, the same test procedure was carried out; however, the part surface was sprayed with a white speckle pattern and evaluated with the software Aramis Professional to capture the full field surface strain. Herein the facet size and point distance are 19 and 16 pixels, as suggested by the producer's instruction. To reduce the measuring noise, the neighborhood strain tensor was two with an increasing reference length for strain calculation, and the spatial median filter was one.[30]

After that, the creep behavior of the SMC part in the aspect of force development was investigated. The test procedure was similar to the above-mentioned one, while the load cell still recorded the force over a delay time of 3600 s, and the cylinder was fixed. The part was measured every 60 s to obtain the surface strain and displacement, respectively. In total, 60 measurements were performed. The cyclic experiments were also performed to characterize the endurance performance of the SMC part. The test procedure was kept the same as the above-mentioned cantilever test; only the loading and unloading process was repeated 50 times. After each cycle, the surface strain and displacement were captured.

Since the measurement accuracy of the strains depends on the testing environment (*e.g.*, illumination, vibration) and set up (*e.g.*, facet size, point distance, strain tensor neighborhood), the optical measurement system was monitored in additionally through the zero-strain deviation.[31,32] In total, 60 frames were measured under the same testing conditions mentioned above. The zero-strain deviation was determined smaller than 0.015%, with a mean of about 0.0075%. For more details, see in (Fig. S3).

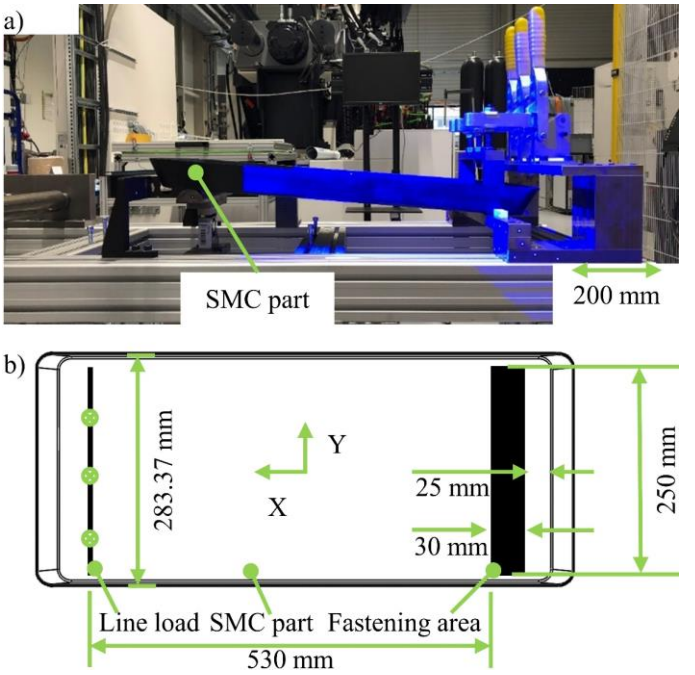

Fig. 4 Test cell with loaded SMC part (a), and a description of the test conditions (b).

3.2 Results and discussions

3.2.1 Bending performance of SMC part

The force control mode was first implemented to characterize the bending behavior of the SMC parts. One typical force-displacement curve of the part with a thickness of 3.3 mm and a weight of 1674 g is presented in Fig. 5a with a resulted cylinder displacement of 41.69 mm, which indicates the deflection of this part at 530 mm from the clamping fixture, illustrated in Fig. 4. Dividing the force by deflection, the global bending stiffness of the part can be calculated.[24] A value of 3.60 N/mm is determined for this SMC part under the loading conditions. In addition, the other 25 SMC parts were

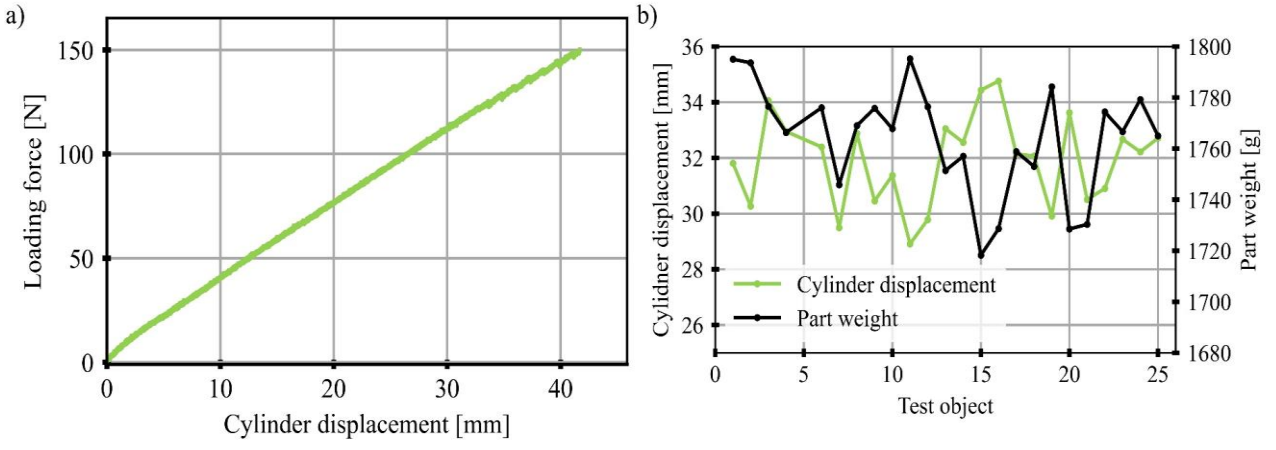

Fig. 5 The exemplary measured force-displacement curve at 530 mm from clamping fixture by the cylinder (a), the relationship between displacement and part weight (b).

also characterized to study the scattering of bending behavior, and the displacements are illustrated in Fig. 5b. It is to be seen that the parts present dominant varied displacement from 28.91 mm to 34.76 mm with a mean of 31.92 mm. The corresponding global bending stiffness varies from 4.32 N/mm to 5.19 N/mm, which is caused by the inconsistent part weight from 1718 g to 1795 g with a mean of 1763.9 g, resulting from the varied weight per unit area of the semi-finished SMC sheets. A negative correlation between the displacement and part weight is proven (heavier part resulting in smaller displacement). The varied part weight leads to difficult lateral contrast in the bending performance.

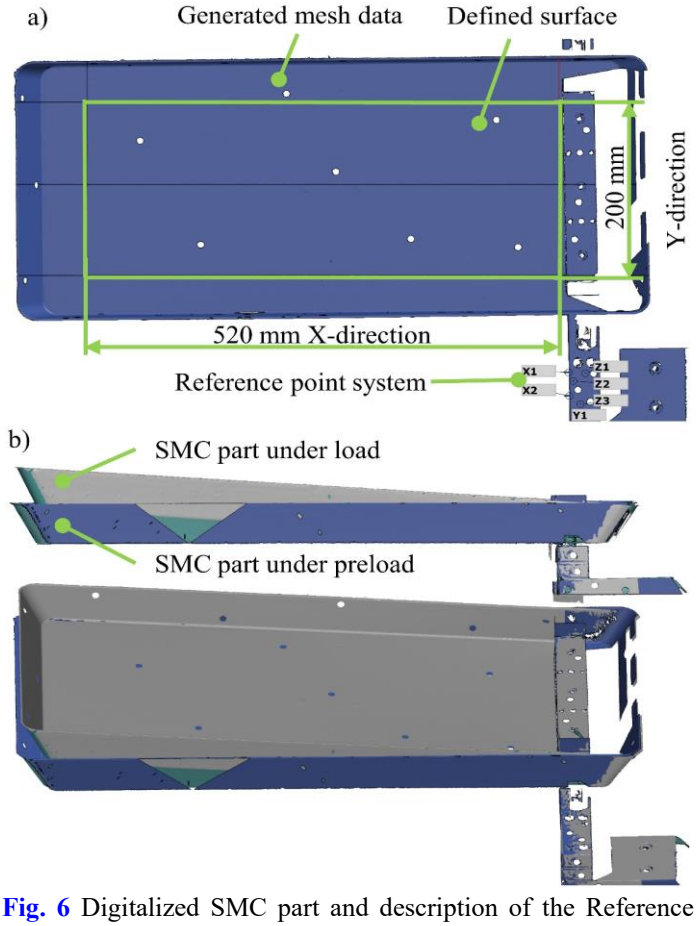

Fig. 6 Digitalized SMC part and description of the Reference Point System (RPS) (a), part difference according to alignment with RPS (b).

To overall and spatially evaluate the bending behavior, the part deformation was fully computed by ATOS 5. After treating the point cloud, the meshes were polygonized generated in STL files and are shown in Fig. 6a. To analyze the part difference, the meshes were aligned with each other with the help of the Reference Point System (RPS) according to Z1, Z2, Z3, X1, X2, and Y1, which was set on the test bench and is also illustrated in Fig. 6a. The resulting part difference is shown in Fig. 6b. Using the ATOS Professional software function, called "surface comparison," the overall part deformation could be presented two-dimensionally. To express more intuitively, one Python script was used. The analysis result is presented in Fig. 7, which describes the part deformation in region 520 × 200 mm (length × width), as shown in Fig. 6a. It is evident that the part positions farther away from the clamping fixture along the X-direction show higher deformation. In addition, the part positions parallel to the clamping fixture along the Y-direction present a similar deformation, meaning without any obvious warpage and a similar stiffness on the part level along this direction.

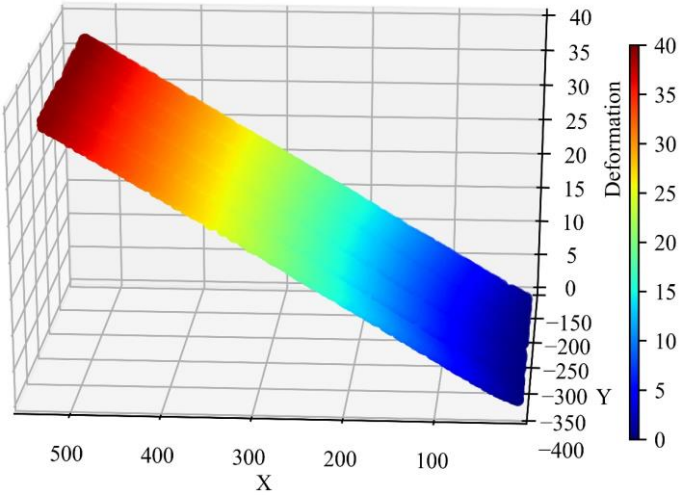

Fig. 7 Overall SMC part deformation in the region 520 × 200 mm in a three-dimensional view.

In terms of spatial properties and the relevant heterogeneity, the full field surface strain was digitalized, and the setup is shown in Fig. 8a. A region of interest (ROI) size of 200 × 200 mm (length × width) was defined. Meanwhile, two cross-sections parallel to the Y-direction were generated. The X-direction strains in the ROI are shown in Fig. 8b with evident spatial dependence. It is to be seen that most areas subject to a low strain between -0.1% and 0.1%, and the positions closer to the clamping fixture subject to higher compressive stress with more significant compressive strains.[33] Exemplary, the average strain in the cross-section1 accounts for -0.21%. However, the positions in the same cross-section present widely different strains in a range of about -0.41% to -0.08%, which is illustrated in Fig. 8c and indicates a substantial spatial heterogeneity of the SMC part. A significant range of fluctuations of the strains and the moduli along cross-section on tensile samples are also determined, with the maximum value being more than twice the minimum value.[34] In addition, some positions in the ROI present positive strains indicating elongation at the spatial positions. The coexistence of tensile and compressive strain is caused by a complex stress condition due to the part side wall, which could be validated with the compressed length of the cross-section2 in the Y-direction by 56 µm from 197.139 mm (before loading) to 197.083 mm (after loading), that should be intrinsically stretched because of the positive Poisson's ratio of SMC.[35] The ROI was compressed both in X- and Y-direction, resulting in spatial elongation and compression coexistence due to heterogeneity.

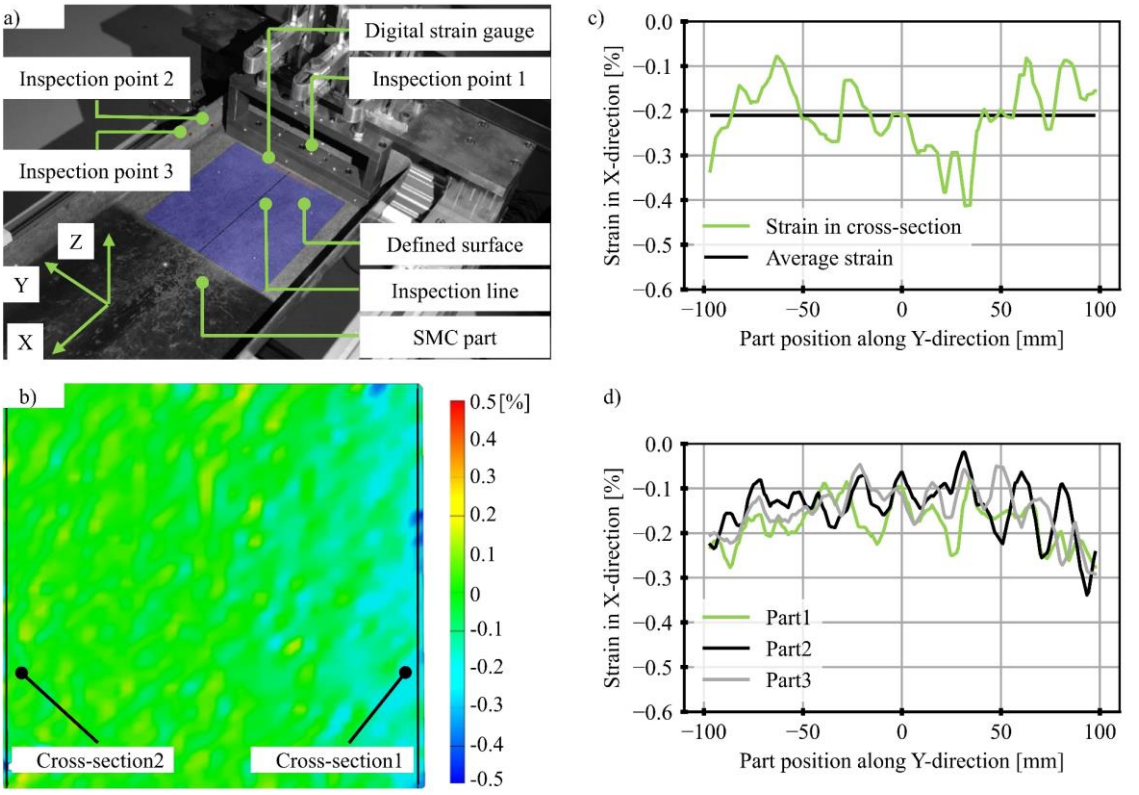

Fig. 8 Analysis of the full field surface strain and heterogeneity, setup of the test (a), determined strain value in the X-direction in the region (b), and in the cross-section1 (c), comparison of part-dependent heterogeneity at the same position (d).

It is worth mentioning that the spatial heterogeneity (strain variation) varies from part to part due to compounding semi-finished sheets and the complex flow behavior in the mold, which is proven by the strain distribution in the cross-section1 of the other three parts, see Fig. 8d. It is to be seen that the exact position of different parts presents different strains (some are the local smallest, and some are the local largest). Dependency of varied modulus distribution on parts was also shown on tensile samples.[10]

3.2.2 Creep performance of SMC part

The creep behavior of the SMC part was investigated as well. Fig. 9a presents the force- and cylinder displacement-loading time curves, which could be divided into two phases: the first is the loading phase to reach the target value, the second represents the delay phase from 91 s to 3691 s under the consistent displacement. Between these two phases, a knee point shows up; after it, the force reduces from 156.8 N to 143.3 N with an attenuation amplitude of 8.6 %. That is, the part creeps under the loading caused plastic deformation. After a pronounced creep close to the knee point, the creep behavior becomes tempered. The two evident creep stages of samples made of SMC were reported as well.[29]

To cross-validate the creep behavior, the surface strain was contactless uninterruptedly measured during the delay, which is evaluated later in X-direction using the digital strain gauge (DMS), one function of the software Aramis. In this work, a digital strain gauge in size of 100 × 10 mm (DMS10) and one cross-section along this DMS were implemented, and the positions are shown in Figs. 8a-b. The average strain and displacement of DMS10 during the delay time are illustrated in Fig. 9b. The average strain increases by 43.1% from -0.167% to -0.239%, and the average displacement keeps nearly constant with a minor change of 5 µm. The locally appeared peaks during loading time could be attributed to the DIC measurement noise.[36,37] The influence of region of interest size is evaluated with a large digital strain gauge measuring 100 × 16 mm (DMS16). The average strain and displacement development are similar to DMS10; more details are given in Fig. S4.

Furthermore, the strains in the cross-section in X-direction at the beginning and end of the creep test are presented in Fig. 9c with a noticeable increase. The strain development is illustrated in Fig. 9d by subtracting the values in the beginning phase from the end phase. Due to material and part creep, the strain increases gradually after reaching a certain force, investigated and proved at the SMC coupon level.[29] Part positions in the cross-section possess different strain development indicating the heterogeneity, and the areas with low strains at the beginning creep obviously. In addition, to cross-over analyze the SMC part's creep behavior, the other 25 SMC parts were characterized, whereby the force remained constant, and the cylinder recorded the displacement over the delay time, which was reduced to 550 s because of the pronounced creep occurring in the initial stage. Two-phase cylinder displacement-loading time curves are presented in Fig. 10, with a loading phase to reach the target force and a delay phase with a continuously increased cylinder

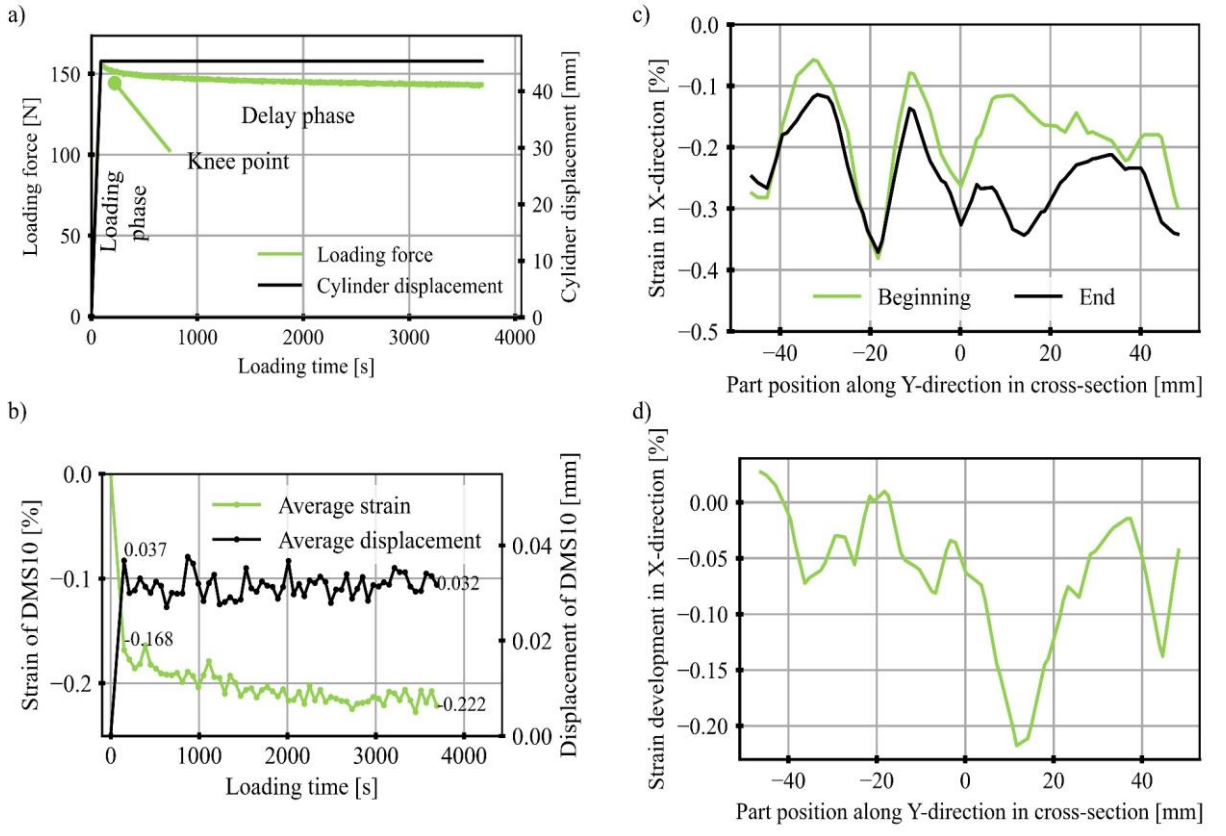

Fig. 9 Diagrams of creep test under constant displacement, force-loading time curve (a), average strain and displacement of DMS 10 (b), strain change in the cross-section at the beginning and end of creep (c), strain development during creep (d).

displacement to compensate for the force attenuation. The increase accounts for between 2.81 mm and 4.59 mm with a mean of 3.66 mm, which indicates an attenuation between 9.7% and 13.3%, with a mean of 11.4%.

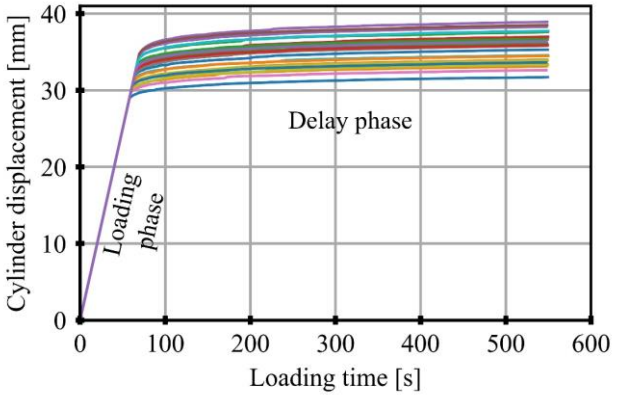

Fig. 10 Displacement-loading time curves of the creep behavior of 25 SMC parts under constant force.

3.2.3 Endurance property of SMC part

The endurance performance of the SMC part was studied under the force control mode. The corresponding force-cylinder displacement curves at the beginning, middle, and end of the loading cycles are depicted in Fig. 11a. It could be seen that the cylinder displacement increases with the loading cycles, and the SMC part in the first cycle subjects a higher force to reach the same displacement compared to the other loading cycles. The virgin SMC part without any loading is stiff and less likely to yield. After the first loading, the microstructure inside the material could be changed, e. g., microcrack and debonding between fiber and matrix, especially when fibers are located vertically to the loading direction,[38,39] which causes mechanical property degradation. After 50 loading cycles, the cylinder displacement increases by 2 mm from 42.5 mm to 44.5 mm with a decreased global bending stiffness of 0.16 N/mm from 3.53 N/mm to 3.37 N/mm. To overall observe the part behavior, the surface strain after each loading cycle was captured using Aramis Professional. One inspection line with a length of 200 mm (Fig. 8a) in X-direction, corresponding to the bending line of the part, was created, and the displacement in Z-direction increases continuously during loading cycles, as shown in Fig. 11b. The increased displacement and corresponding degraded stiffness under alternative loading also exist at the coupon level.[40]

Similar to the above mentioned, the digital strain gauge DMS10 is used to evaluate the endurance performance according to the average strain in X-direction and the displacement. Meanwhile, inspection point 1 was also created to inspect the movement of the clamping fixture during cycle loading, which is described in (Fig. 8a). The measurement results of these three parameters are shown in (Fig. 12a). It can be seen that the average strain of DMS10 has almost no

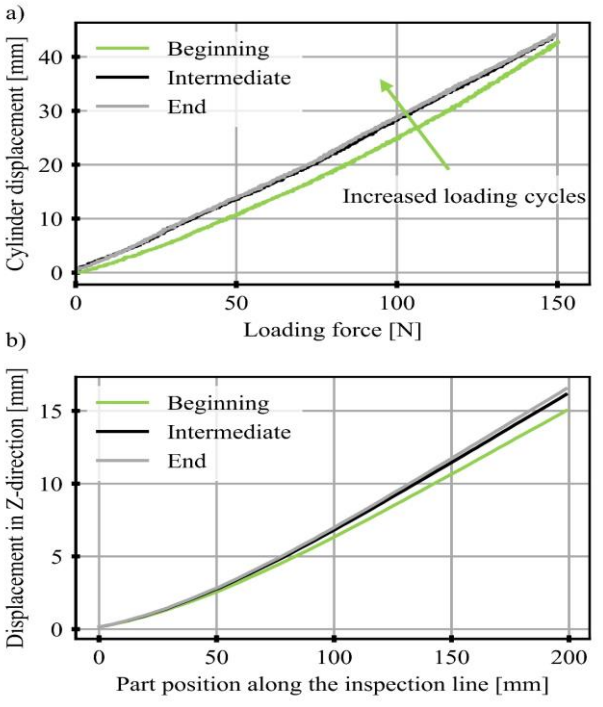

Fig. 11 Diagrams of an endurance test, force-cylinder displacement curves (a), displacement of inspection line in the Z-direction (b).

change between -0.17% (at the first measuring stage) and -0.18% (at the last measuring stage). The average displacement of DMS10 increases slightly from 0.27 mm to 0.38 mm, which could be caused either by the deterioration of the SMC part due to plastic deformation or by a loose clamping fixture. The latter is excluded as a root cause, after analyzing the displacement of the inspection point on the clamping fixture, which keeps constant at 0.01 mm.

To evaluate the endurance performance of this SMC part, the side wall area close to the clamping fixture is analyzed using two inspection points (isp), 2 and 3, as shown in (Fig. 8a). The distance between these two points in the X-direction decreases from 41.26 mm (before loading) to 41.17 mm (after the first loading) and 41.13 mm (after the last loading) with a strain of about -0.31%, which means that these two points move to each other with an increased curvature in this side wall area, as illustrated in Fig. 12b. The displacement of the inspection line is investigated in the X- direction as well. As presented in Fig. 12c, the displacement of the end of the inspection line, which is near to clamping fixture, exhibits almost no change (0.115 mm at the beginning and 0.129 mm at the end). In contrast, the other end shows an apparent displacement (-0.494 mm at the beginning and -0.595 mm at the end). These two ends are getting closer during loading with an increased curvature, similar to the phenomenon in the side wall area. It is concluded that the local area under high stress degrades gradually during cyclic loading. Spatial material properties decide the changing of microstructure under loading, *e.g.*, crack initiation and propagation.[10]

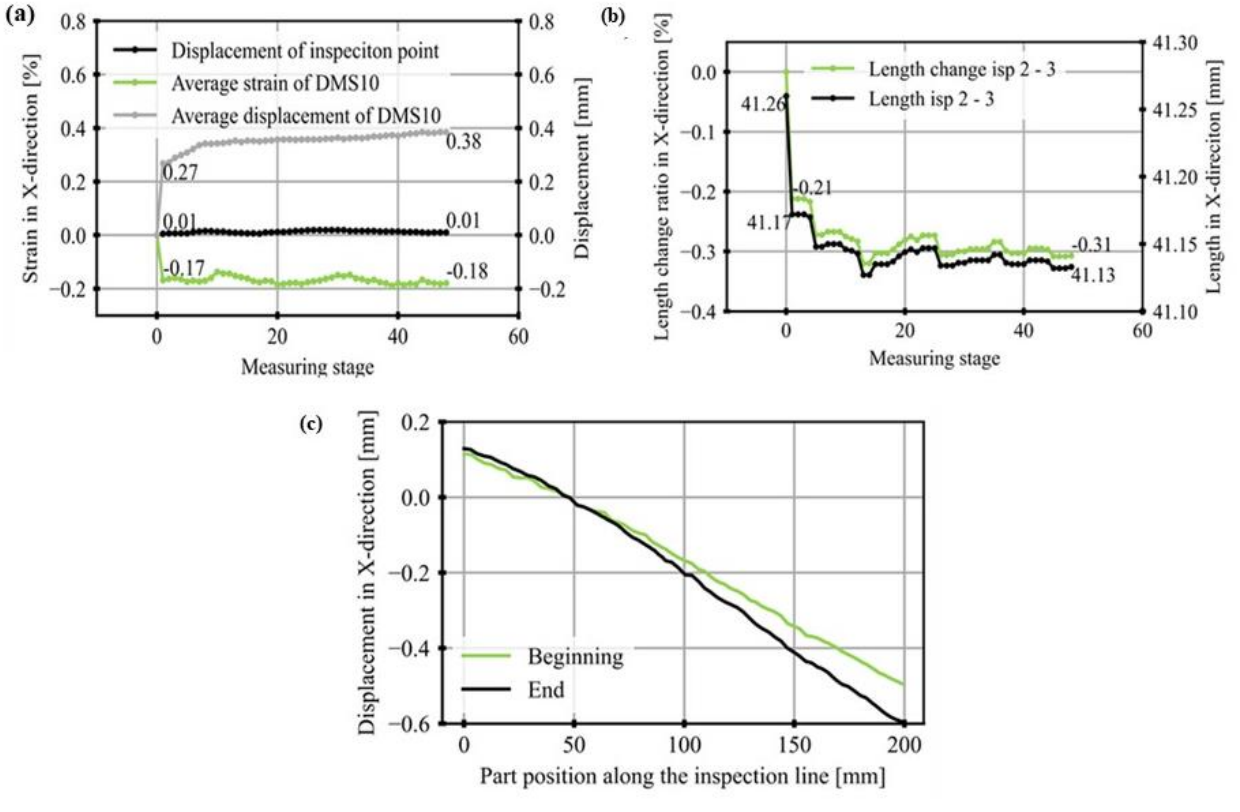

Fig. 12 Analysis of endurance performance, average strain, and displacement of DMS10 as well as displacement of clamping fixture (a), length change between inspection point (isp) 2 and 3 located in the side wall (b), displacement of inspection line in the X-direction (c).

4. Conclusions

To easily investigate the heterogeneity of the SMC part with consideration of the spatial morphology without testing any local samples, a more accessible and faster-operated test cell was developed, designed, and investigated. The part geometry, deformation, and surface strain could be digitalized with high accuracy (mean zero strain deviation of about 0.0075%). The test cell is flexible to adapt to the other parts (investigating the complex geometrical part is illustrated in Fig. S5). One unique platform for real-time finite element analysis was integrated to provide a virtual overall part performance. Divers load cases were realized through displacement- and force-control mode with configurable parameters, *e.g.*, force, velocity, displacement, loading cycle, and delay time.

Different tests were conducted to characterize the SMC parts' performance, including bending behavior with inspection of part deformation and strain considering the spatial properties, creep behavior, and endurance performance. Strain values of about -0.41% to -0.08% on the cross-section perpendicular to the material flow direction are shown. Besides, the SMC parts creep gradually with two stages, both under constant deformation and loading force, resulting in a decreased force by 8.6% and increased displacement by 11.4%, respectively. Higher stiffness of the virgin SMC part without any loading is shown under the endurance test. The part degrades gradually within 50 cycles with a decreased bending stiffness by 4.5% and increased curvature in the highly stressed area.

In summary, SMC parts' bending and creep behavior and endurance performance considering heterogeneity are evaluable at this test cell. The heterogeneity can be identified and statistically quantified using the first load case, while the second load case indicates creep happens mainly in the local areas with high stiffness. The third load case points out that the heterogeneity in the area under high stress must be deeply evaluated and inspected as SMC parts in service.

Acknowledgements

This work was supported by the state North Rhine-Westphalia with the framework of European Regional Development Fund (No.: EFRE-0801116) and managed by the Project Management Agency Jülich (PTJ), to whom we would like to express our gratitude. We extend our sincere thanks to AOC Aliancys for the provided equipment support.

Conflict of Interest

The authors declare no conflict of interest.

Supporting information

Applicable

References

[1] M. Shirinbayan, H. B. Rizi, N. Abbasnezhad, A. Tcharkhtchi, J. Fitoussi, Tension, compression, and shear behavior of advanced sheet molding compound(A-SMC): Multi-scale damage analysis and strain rate effect, *Composites Part B: Engineering*, 2021, **225**, 109287, doi: 10.1016/j.compositesb.2021.109287.

[2] P. Feraboli, T. Cleveland, P. Stickler, J. Halpin, Stochastic laminate analogy for simulating the variability in modulus of discontinuous composite materials, *Composites Part A: Applied Science and Manufacturing*, 2010, **41**, 557-570, doi: 10.1016/j.compositesa.2010.01.003.

[3] M. Shirinbayan, Multiscale damage analysis of the tension-tension fatigue behavior of a low-density sheet molding compound, *Journal of Applied Polymer Science*, 2021, **138**, 49721, doi: 10.1002/app.49721.

[4] F. Gortner, A. Schueffler, J. Fischer-Schuch, P. Mitschang, Use of bio-based and renewable materials for sheet molding compounds(SMC) mechanical properties and susceptibility to fungaldecay, *Composites Part C: Open Access*, 2022, **7**, 100242, doi: 10.1016/j.jcomc.2022.100242.

[5] M. Schemmann, J. Lang, A. Helfrich, T. Seelig, T. Boehlke, Cruciform specimen design for biaxial tensile testing of SMC, *Journal of Composites Science*, 2018, **2**, 12, doi: 10.3390/jcs2010012.

[6] N. E. J. Olsson, T. S. Lundström, K. Olofsson, Design of experiment study of compression moulding of SMC, *Plastics Rubber and Composites*, 2009, **38**, 426-431, doi: 10.1179/146580109x12540995045886.

[7] P. Dumonz, L. Orgéas, D. Favier, P. Pizette, C. Venrt, Compression moulding of SMC : In situ experiments, modelling and simulation, *Composites Part A: Applied Science and Manufacturing*, 2007, **38**, 353-368, doi: 10.1016/j.compositesa.2006.03.010.

[8] P. Feraboli, E. Peitso, F. Deleo, T. Cleveland, Characterization of prepreg-based discontinuous carbon fiber/epoxy systems, *Journal of Reinforced Plastics and Composites*, 2009, **28**, 1191-1214, doi: 10.1177/0731684408088883.

[9] P. Feraboli, E. Peitso, T. Cleveland, P. B. Stickler, J. C. Halpin, Notched behavior of prepreg-based discontinuous carbon fiber /epoxy systems, *Composites Part A: Applied Science and Manufacturing*, 2009, **40**, 289-299, doi: 10.1016/j.compositesa.2008.12.012.

[10] H. Tang, Z. X. Chen, G. Zhou, Y. Li, K. Avery, H. D. Guo, H. Kang, D. Zeng, X. M. Su, Correlation between failure and local material property in chopped carbon fiber chip-reinforced sheet molding compound composites under tensile load, *Polymer Composites*, 2018, **40**, 962-974, doi: 10.1002/pc.24767.

[11] Z. X. Chen, H. B. Tang, Y. M. Shao, Q. P. Sun, G. W. Zhou, Y. Li, H. Y. Xu, D. Zeng, X. M. Su, Failure of chopped carbon fiber sheet molding compound(SMC) composites under uniaxial tensile loding : Computational prediction and experimental analysis, *Composites Part A: Applied Science and Manufacturing*, 2019, **118**, 117-130, doi: 10.1016/j.compositesa.2018.12.021.

[12] M. A. Laribi, R. TieBi, S. Tamboura, M. Shirinbayan, A. Tcharkhtchi, H. B. Dali, J. Fitoussi, Sheet molding compound automotive component reliability using a micromechanical damage approach, *Applied Composite Materials*, 2020, **5**, 693-

715, doi: 10.1007/s10443-020-09831-5.
[13] A. Trauth, P. Pinter, K. Weidenmann, Investigation of quasi-static and dynamic material properties of a structural sheet molding compound combined with acoustic emission damage analysis, *Journal of Composites Science*, 2017, **1**, 18, doi: 10.3390/jcs1020018.
[14] N. Meyer, L. Schöttl, L. Bretz, A. Hrymak, L. Kärger, Direct bundle simulation approach for the compression mloding process of sheet molding compound, *Composites Part A: Applied Scicence and Manufacturing*, 2020, **132**, 105809, doi: 10.1016/j.compositesa.2020.105809.
[15] C. Hopmann, J. Neuhaus, K. Fischer, D Schneider, R. L. P. Gonçalves, Metamodelling of the correlations of preform and part performance for preform optimisation in sheet moulding compound processing, *Journal of Composites Science*, 2020, **4**, 122, doi: 10.3390/jcs4030122.
[16] J. Görthofer, N. Meyer, T. D. Pallicity, L. Schöttl, A. Trauth, M. Schemmann, M. Hohberg, P. Pinter, P. Elsner, F. Henning, A. Hrymak, T. Seelig, K. Weidenmann, L Kärger, T. Böhlke, Motivating the development of a virtual process chain for sheet molding compound composites, *Proceedings in Applied Mathematics and Mechanics*, 2019, **19**, e201900124, doi: 10.1002/pamm.201900124.
[17] Z. X. Chen, T. Y. Huang, Y. M. Shao, Y. Li, H. Y. Xu, K. Avery, D. Zeng, W. Chen, X. M. Su, Multiscale finite element modeling of sheet molding compound (SMC) composite structure based on stochastic Mesostructure Reconstructio, *Composite Structures*, 2018, **188**, 25-38, doi: 10.1016/j.compstruct.2017.12.039.
[18] Y. Z. Li, S. Pimenta, J. Singgih, S. Northdurfter, K. Schuffenhauer, Experimental investigation of randomly-oriented two-based discontinuous composites and their equivalent laminates, *Composites Part A: Applied Science and Manufacturing*, 2017, **102**, 64-75, doi: 10.1016/j.compositesa.2017.06.031.
[19] F. Rothenhäusler, N. Meyer, S. Wehler, M. Hohberg, M. Gude, F. Henning, L. Kärger, Experimental and Numerical analysis of SMC compression molding in confined regions-A comparison of simulation approaches, *Journal of Composites Science*, 2022, **6**, 68, doi: 10.3390/jcs6030068.
[20] M. Hohberg, L. Kärger, F. Henning, A. Hrymak, Rheological measurements and rheological shell model considering the compressible behavior of long fiber reinforced sheet molding compound (SMC), *Composites Part A: Applied Science and Manufacturing*, 2017, **95**, 110-117, doi: 10.1016/j.compositesa.2017.01.006.
[21] S. Boylan, J. M. Castro, Effect of reinforcement type and length on physical properties, surface quality, and cycle time for sheet molding compound (SMC) compression molded parts, *Journal of Applied Polymer Science*, 2003, **90**, 2557-2571, doi: 10.1002/app.12726.
[22] A. Trauth, M. Bondy, K. A. Weidenmann, W. Altenhof, Mechanical properties and damage evolution of a structural sheet molding compound based on a novel two step curing resin system, *Materils and Design*, 2018, **143**, 224-237, doi: 10.1016/j.matdes.2018.02.002.
[23] L. M. Martulli, T. Creemers, E. Schöberl, N. Hale, M. Kerschbaum, S. V. Lomov, Y. Swolfs, A thick-walled sheet moulding compound automotive component: manufacturing and performance, *Composites Part A: Applied Science and Manufacturing*, 2020, **128**, 105688, doi: 10.1016/j.compositesa.2019.105688.
[24] M. Oldenbo, D. Mattson, J. Varna, L. A. Berglund, Global stiffness of a SMC panel considering process induced fiber orientation, *Journal of Reinforced Plastics and Composites*, 2004, **23**, 37-49, doi: 10.1177/0731684404028700.
[25] P. Feraboli, E. Peitso, T. Cleveland, Modulus measurement for prepreg-based discontinuous carbon fiber/epoxy systems, *Journal of Composites Materials*, 2009, **43**, 1947-1965, doi: 10.1177/0021998309343028.
[26] M. Piry, W. Michaeli, Stiffness and failure analysis of SMC components considering the anisotropic material properties, *Macromolecular Materials Science and Engineering*, 2000, **284**, 40-45, doi: 10.1002/1439-2054(20001201).
[27] D. Palousek, M. Omasta, D. Koutny, J. Bednar, T. Koutecky, F. Dokoupil, Effect of matte coating on 3D optical measurement accuracy, *Optical Materials*, 2015, **40**, 1-9, doi: 10.1016/j.optmat.2014.11.020.
[28] D. Pan, G. Yang, H.M. Abo-Dief, J. Dong, F. Su, C. Liu, Y. Li, B. Bin Xu, V. Murugadoss, N. Naik, S.M. El-Bahy, Z.M. El-Bahy, M. Huang, Z. Guo, Vertically aligned silicon carbide nanowires/boron nitride cellulose aerogel networks enhanced thermal conductivity and electromagnetic absorbing of epoxy composites, *Nano-Micro Letters*, 2022, **14**, 118, doi: 10.1007/s40820-022-00863-z.
[29] D. Finck, C. Seidel, A. Ostermeier, J. Hausmann, T. Rief, Experimental investigation on the in-plane creep behavior of a carbon-fiber sheet molding compound at elevated temperature at different stress states, *Materials*, 2020, **13**, 2545, doi: 10.3390/ma13112545.
[30] N. S. Ha, T. Jin, N. S. Goo, Modal analysis of an artificial wing mimicking an Allomyrina dichotoma beetle's hind wing for flapping-wing micro air vehicles by noncontact measurement techniques, *Optics and Lasers in Engineering*, 2013, **51**, 560-570, doi: 10.1016/j.optlaseng.2012.12.012.
[31] A. Fathi, J.-H. Keller, V. Altstaedt, Full-field shear analyses of sandwich core materials using digital image correlation (DIC), *Composites Part B: Engineering*, **70**, 156-166, doi: 10.1016/j.compositesb.2014.10.045.
[32] G. L. Golewski, Evaluation of fracture processes under shear with the use of DIC technique in fly ash concrete and accurate measurement of crack path lengths with the use of a new crack tip tracking method, *Measurement*, 2021, **181**, 109632, doi: doi.org/10.1016/j.measurement.2021.109632.
[33] S. I. A. Jalali, P. Kumar, V. Jayaram, High throughput determination of creep parameters using cantilever bending: part i-steady-state, *Journal of Materials Research*, 2020, **35**, 353-361, doi: 10.1557/jmr.2020.36.
[34] X. Sun, C. Engler-Pinto, L. Huang, S. Y. Huang, H. B. Tang, H. T. Cui, X. M. Su, Investigation of mechanical behavior of

chopped carbon fiber reinforced sheet molding compound (SMC) composites, *SAE Technical Papers*, 2020, **1**, 1307, doi.org/10.4271/2020-01-1307.
[35] J. Görthofer, G. Schneider, F. Ospald, A. Hrymak, T. Böhlke, Computational homogenization of sheet molding compound composites based on high fidelity representative volume elements, *Computational Materials Science*, 2020, **174**, 109456, doi: 10.1016/j.commatsci.2019.109456.
[36] M. Selezneva, L. Lessard, Characterization of mechanical properties of randomly oriented strand thermoplastic composites, *Journal of Composites Materials*, 2015, **50**, 2833-2851, doi: 10.1177/0021998315613129.
[37] B. Pan, H. Xie, Z. Wang, K. Qian, Z. Wang, Study on subset size selection in digital image correlation for speckle patterns, *Optices Express*, 2008, **16**, 7037-7048, doi: 10.1364/OE.16.007037.
[38] J. Görthofer, N. Meyer, T. D. Pallicity, L. Schöttl, A. Trauth, M. Schemmann, M. Hohberg, P. Pinter, P. Elsner, F. Henning, A. Hrymak, T. Seelig, K. Weidenmann, L. Kärger, T. Böhlke, Virtual process chain of sheet molding compound: development, validation and perspectives, *Composites Part B: Engineering*, 2019, **169**, 133-147, doi: 10.1016/j.compositesb.2019.04.001.
[39] M. Shirinbayan, J. Fitoussi, M. Bocquet, F. Meraghni, B. Surowiec, A. Tcharkhtchi, Multi-scale experimental investigation of the viscous Molding Compound(A-SMC) subsitted to high strain rates, *Composites Part B: Engineering* , 2017, **115**, 3-13, doi: 10.1016/j.compositesb.2016.10.061.
[40] D. Finck, C. Seidel, J. Hausmann, T. Rief, Creep-induced screw preload loss of carbon - fiber sheet molding compound at elevated temperature, *Materials*, 2019, **12**, 3598, doi: 10.3390/ma12213598.

Author Information

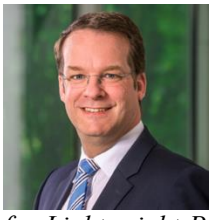

Prof. Christian Hopmann *holds the Chair for Plastics Processing and is director of the IKV – Institute for Plastics Processing in Industry and Crafts at RWTH Aachen University in Germany. He is co-founder of the AZL – Aachen Center for Lightweight Production and Vice Dean of the faculty for Mechanical Engineering of RWTH Aachen University. His interest is fundamental and applied research in plastics technology with a particular focus on Digitization and Simulation, Lightweight Technologies and Circular Economy. Professor Hopmann is principal investigator and member of the steering committee of the Federal Cluster of Excellence "Internet of Production". He initiated the Polymer Innovation Center 4.0, which addresses the domain-specific realization and implementation of digitization in the plastics industry with a particular focus on SMEs. After studying mechanical engineering, he received his doctoral degree from RWTH Aachen University. Following a senior vice-director position at IKV, he started his industrial career in 2005 at the plastics processing company RKW SE, latterly as Managing Director of RKW Sweden A.B. in Helsingborg. He participated in the program for executive development at the International Institute for Management Development (IMD) in Lausanne, Switzerland. Hopmann received the Innovation Award of Germany's federal state North Rhine Westphalia in 2014. He was appointed visiting professor at the Beijing University of Chemical Technology, Beijing/China, in 2017 and a fellow of the Society of Plastics Engineers, CT/USA, in 2019. Hopmann serves as international representative of the Polymer Processing Society since 2021 and is a member of the board of directors and the scientific advisory board as well as chairman of the board of the material engineering division of the VDI – The Association of German Engineers since 2022.*

Hao Wang*, a research assistant at the Aachen Center for Integrative Lightweight Production (AZL) and a PhD student in the faculty of mechanical engineering at RWTH Aachen University since 2018. He is the workgroup leader for Advanced Thermoset Production at AZL Aachen GmbH. He is engaged in process-structure-property-performance of hybrid composites.*

Markus Breiing *studied at RWTH Aachen University, Aachen, Germany, and at UPV Valencia, Valencia, Spain, and holds a bachelor's and a master's degree in mechanical engineering and business administration. He is pursuing his PhD in lightweight production under Prof. Hopmann at RWTH Aachen University. He is also head of the Business Unit Digitalization & Technology Evaluation at Conbility GmbH and focuses on the economic and ecological assessment of composite process chains.*

Kai Fischer *studied mechanical engineering with a focus on aerospace engineering at RWTH Aachen University. He obtained his doctorate with honors in high-volume production of components made of fiber-reinforced plastics with thermoset matrix. As Scientific Director at the Institute for Plastics Processing (IKV) at RWTH Aachen University, he is responsible for the strategic planning and cross-departmental coordination of all technologies related to lightweight engineering. He is also a member of the management board of the Aachen Center for Integrative Lightweight Production (AZL) of RWTH Aachen University and managing director of AZL Aachen GmbH, a provider of services for business and technology development in the field of lightweight engineering and strategic consulting. Dr Fischer has published approximately 200 publications as an author and is a lecturer at RWTH Aachen University for the lecture "Fiber Reinforced*

Composites". Dr Fischer's work has been honored by the Society for the Advancement of Materials and Process Engineering (SAMPE), several times the German Federation of Reinforced Plastics (AVK), the Future Award of the State of North Rhine Westphalia (the highest donated German award for applied science behind the German Future Award), the JEC Innovation Award and the Borchers Badge.

***Dr. Michael Emonts**, born in 1977, studied mechanical engineering at the RWTH Aachen University, focusing on production engineering. He completed his doctoral studies with distinction in 2010. From April 2005 to September 2007, he worked as a research assistant at the Fraunhofer Institute for Production Technology IPT in the Production Machines department. Furthermore, from October 2007 to December 2009, he was group leader of the group "Fiber Composite and Laser Systems Technology", where he was responsible for the development of tape placement and tape winding machines for laser-assisted tape processing with in-situ consolidation. From January 2010 until the end of 2016, Dr Emonts headed the department "Composite Fiber and Laser Systems Technology" at the Fraunhofer IPT as Chief Engineer. Since 2012 Dr Emonts has been Managing Director of the Aachen Center for Integrative Lightweight Production (AZL) of RWTH Aachen University and is also Managing Partner of AZL Aachen GmbH, a provider of industrial services in the field of lightweight construction technology and strategic consulting with an international industrial network of more than 80 partner companies. In addition, Since January 2015, Dr Emonts has been Co-Founder and Managing Partner of Conbility GmbH, a supplier of tape placement machines, among others. Dr Emonts has received several prestigious awards for his work, including the Borchers Badge of the RWTH Aachen University, the MM Award, the Ferchau Innovation Award, and several times the international JEC World Innovation Award in Paris. Since 2016 he has been a lecturer at RWTH Aachen University: he initiated, conceptualized and supervised the lecture "Lightweight Production Systems -LeiPro" and is the author of more than 100 publications.*

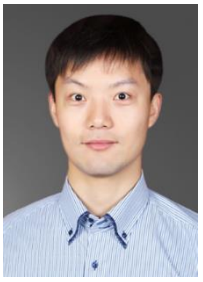

***Jian Wang** is currently a professor at the Beijing University of Chemical Technology, China. He has received the Humboldt Research Fellowship for experienced researchers. He has served as a fellow of the China Plastic Processing Industry Association (CPPIA) (Board of Directors, both of the Injection Molding Products Committee and the Plastics Technology Collaboration Committee) and a fellow of the CAE Molding Solution Alliance of China. He has been working in the science and engineering of polymer processing, especially on injection moulding, extrusion, and polymer composites.*

